Journal of Environmental Chemical Engineering 11 (2023) 109724

Contents lists available at ScienceDirect

Journal of Environmental Chemical Engineering

journal homepage: www.elsevier.com/locate/jece

# Optimized manufacturing of gas diffusion electrodes for $CO_2$ electroreduction with automatic spray pyrolysis

Jose Antonio Abarca [a,*], Guillermo Díaz-Sainz [a], Ivan Merino-Garcia [a], Garikoitz Beobide [b,c], Jonathan Albo [a], Angel Irabien [a]

[a] Departamento de Ingenierías Química y Biomolecular, Universidad de Cantabria, ETSIIT, Avenida de los Castros 46, 39005, Santander, Spain
[b] Department of Organic and Inorganic Chemistry, University of the Basque Country, UPV/EHU, P.O. 644, Bilbao E-48080, Spain
[c] BCMaterials, Basque Center for Materials, Applications and Nanostructures, UPV/EHU Science Park, Leioa 48940, Spain

ARTICLE INFO

Editor: Despo Kassinos

*Keywords:*
$CO_2$ electroreduction
Gas diffusion electrodes
Electrode manufacturing
Spray pyrolysis
Plasma surface treatment
Formate

ABSTRACT

Despite being one of the most promising $CO_2$ utilization strategies some aspects still hinder the scaling up of $CO_2$ electroreduction processes. One of them is the fabrication of the electrodes, which is currently rudimentary and depends fundamentally on the human factor. Here, we report an automated spray pyrolysis technique coupled with a plasma surface treatment to fabricate Bi-based gas diffusion electrodes for a enhanced $CO_2$ electroreduction to formate. Three fabrication parameters, namely i) spraying nozzle height, ii) step distance, and iii) ink flow rate, are evaluated to determine the optimal fabrication conditions. The results confirm the reproducibility of the fabrication method, improving the overall performance of the electrodes fabricated with a manual airbrushing method, and leading to formate rates of up to 10.1 mmol $m^{-2}$ $s^{-1}$ at 200 mA $cm^{-2}$. Besides, plasma treatment can improve formate concentration by up to 12 % in comparison with the untreated electrode. As a result, this work provides novel insights into the development of more efficient methods to manufacture electrodes for $CO_2$ electroreduction, which will eventually bring this technology closer to an industrial scale.

## 1. Introduction

Several approaches can be considered to reduce $CO_2$ emissions in different economic sectors, including developing renewable energy sources, enhancing the energy efficiency of buildings, or decarbonization by means of electrification [1]. Some industrial processes, however, cannot avoid the generation of $CO_2$. In this regard, $CO_2$ capture, utilization, and storage (CCUS) can be considered one of the most promising mitigation strategies [2].

Among the different available approaches, the electrochemical reduction of $CO_2$ stands out as one of the most efficient utilization and conversion technologies, since it can store the energetic excess from intermittent and renewable sources of energy in form of chemical bonds, leading to different value-added products such as formic acid/formate ($HCOOH/HCOO^-$), methanol ($CH_3OH$), ethanol ($C_2H_5OH$), or ethylene ($C_2H_4$), among others [3]. In particular, formate is an appealing reduction product that can be considered one of the closest chemicals for future implementation of $CO_2$ electroreduction at an industrial scale [4–6]. Formate finds application in different industries as raw materials (e.g., leather tanning, animal feed, or pharmaceutical), and has also gained attention as a hydrogen carrier and reactant for low-temperature fuel cells [5]. In recent years, great advances have been achieved in the electrochemical $CO_2$-to-formate process in terms of (i) development of reactor configurations [7–11], (ii) electrode morphology [12–17], (iii) synthesis and characterization of electrocatalysts [18–22], and (iv) analysis of operating conditions [9–11,23]. Despite this, the actual Technological Readiness Level (TRL) for this process is between 3 and 5 [24], which is still far from an industrial scale-up. To get closer to real applications, the research should be focused, not only on efficient materials [25] and reactors [26], but also on the development of optimized protocols for electrode manufacturing and in particular for Gas Diffusion Electrodes (GDEs), where an enhanced performance can be achieved due to better contact between the reactive gas, the catalyst, and the electrolyte [27]. $CO_2$ reduction with GDEs is sensitive to alterations in the wettability, porosity, and morphology of the electrodes according to a previous report [28], thus making the manufacturing reproducibility of GDEs a major challenge. These alterations seem to be related to the loadings and spatial distributions of both the catalyst particles and the

* Corresponding author.
*E-mail address:* joseantonio.abarca@unican.es (J.A. Abarca).

https://doi.org/10.1016/j.jece.2023.109724
Received 6 February 2023; Received in revised form 10 March 2023; Accepted 16 March 2023
Available online 17 March 2023

ionomer that acts as the binder [29], attributed to phase segregation during the electrode manufacturing process [30]. In this line, previous results in our research group denoted the significant difference in the formate rates achieved with GDE-based electrodes prepared by a manual airbrushing method [8,11,17,23]. The relative standard deviations (RSD) reached for formate rates were as high as 15 %, which clearly supports the need to develop reproducible and dedicated GDE fabrication techniques.

Among the different GDE manufacturing methods, including sputtering techniques [31], electroplating [32], or chemical vapor deposition [33], spray deposition emerges as an efficient and fast technique for the deposition of thin catalytic layers on electrode substrates [34]. One of the most widely-used spray coating techniques is airbrushing; however, its manual operation directly relies on the human factor, causing non-reproducible electrode properties such as thickness and homogeneity [35,36]. Thus, other advanced spray-coating techniques, such as spray pyrolysis, should be employed to manufacture scalable GDEs with less material use and high homogeneity in an automated process [37]. Some of the most important variables in the operation of a spray pyrolysis technique are the ink flow rate, the nozzle height, the step distance, the deposition rate, or the hot plate temperature, where all of them may define the morphology of the fabricated electrode [38], and thus the overall electrode performance. Previous works that employ for GDEs fabrication an automatic spray pyrolysis technique are focused on studying the influence of different ink solvents [39] and the layer composition[29], or comparing the deposition uniformity versus other fabrication techniques [40]. However, as far as the authors know, the impact of the fabrication variables on the GDE performance for the electroreduction of $CO_2$ has not been studied in detail yet.

Moreover, literature shows that GDEs can undergo a surface modification for an enhanced $CO_2$ electroreduction performance [41–45], where plasma surface treatment offers operational versatility and promising results due to physical or chemical modification of the surface and the first layers of the treated material. The overall properties of the initial structure are maintained [46,47], while enabling the fine-tuning of several properties of the metal catalyst such as chemical state [48], ion content [49], or surface roughness [50], among others.

All in all, the main objective of this work is to optimize the GDEs manufacturing process by applying an automated fabrication technique based on spray pyrolysis, combined with a superficial atmospheric plasma post-treatment. This may help to advance the development of electrode manufacturing processes that approach $CO_2$ electroreduction to industrial-scale implementation. The analyses include reproducibility tests and evaluation of different fabrication variables, namely nozzle height, distance between steps, and ink flow rate with influence on formate rate and energy consumption. The results are discussed together with electrochemical and physicochemical characterization results, including thickness, internal structure, charge resistance, surface hydrophilicity, or chemical state.

## 2. Methodology

### 2.1. Electrode manufacturing with automatic spray pyrolysis

A commercial ND-SP Mini Ultrasonic Spray Coater (Nadetech Innovations) is used for the fabrication of the GDEs. The system consists of a heating plate on which the electrode support is placed, a syringe-shaped ink reservoir, an ultrasonic dispersion system, and a spraying nozzle that allows the automated manufacturing of electrocatalytic surfaces. The heating plate temperature is 70 ºC to ensure the evaporation of isopropanol, and to avoid the degradation of the polymeric materials (Nafion).

The GDEs (10 $cm^2$ – geometric area) are composed of three separated layers: (i) carbonaceous support, Toray TGP-H 60 (Alfa Aesar), (ii) a microporous layer (MPL), formed by Vulcan XC 72-R (Cabot) and PTFE (60 % wt., Sigma Aldrich), with high conductivity and chemical resistance, with a 2 mg $cm^{-2}$ loading, and (iii) the catalytic layer (CL), with a loading of 0.75 mg $cm^{-2}$. Bi carbon-supported nanoparticles are employed as a non-precious metal electrocatalyst, whose synthesis and characterization can be found in detail elsewhere [11,17], as well as the ink formulation for both MPL and CL [9,11,23]. The ink viscosity is estimated to be approximately 2.4 cP, owing to the presence of isopropanol as the solvent (97 wt%). It is worth mentioning that decreasing the ink viscosity may lead to a reduced electrode thickness, as the catalyst is likely to be deposited more efficiently within the pores of the MPL [51].

The effect of the following fabrication variables on electrode performance is studied: (i) the spraying nozzle height (15, 25, and 35 mm), (ii) the step distance (1 and 3 mm), which is the inter-pass distance over the electrode surface left by the nozzle, and (iii) the ink flow rate (10 and 20 ml $h^{-1}$). A schematic representation of these three fabrication variables is displayed in Supporting Information (Fig. S1). Other fabrication parameters, such as the compressed air pressure (0.3 bar), and the spraying nozzle speed (400 mm $min^{-1}$) are set in all cases to ensure the correct dispersion of the material.

### 2.2. Plasma surface treatment

Subsequently, the surfaces of the prepared GDEs are treated with air-based low-pressure plasma equipment (Piezo brush® PZ3, Reylon plasma) for 30 s to ensure the correct surface treatment, as depicted in the literature [49]. Different treatments are evaluated: i) treatment of the supporting Toray layer, ii) treatment of both, the supporting layer and the MPL, and iii) treatment of all layers, namely the supporting layer, the MPL, and the CL.

### 2.3. Performance in a filter-press reactor and electrochemical characterization

The manufactured GDEs are tested as cathodes in a two-compartment filter press electrochemical reactor (Micro Flow Cell, ElectroCell A/s), at ambient temperature and pressure conditions (please see Fig. S2 in the Supporting Information (SI)).

Pure gas $CO_2$ is fed to the cathodic compartment with a flow rate of 200 ml $min^{-1}$, together with a liquid catholyte with a composition of 0.5 M KCl (Potassium Chloride, pharma grade, PanReac AppliChem) + 0.45 M $KHCO_3$ (Potassium Bicarbonate, pharma grade, PanReac AppliChem) at a flow rate per geometric surface area of 0.57 ml $min^{-1}$ $cm^{-2}$. A commercial dimensionally stable anode [DSA/$O_2$ (Ir-MMO (Mixed Metal Oxide) on platinum), ElectroCell] is employed as the counter electrode to carry out the oxygen evolution reaction, and the liquid anolyte consists of an aqueous solution 1 M KOH (Potassium Hydroxide, 85 % purity pellets, PanReac AppliChem), fed with a flow rate per geometric surface area of 0.57 ml $min^{-1}$ $cm^{-2}$, in line with previous studies [17]. A leak-free Ag/AgCl 3.4 M KCl electrode is used as the reference electrode. Both compartments are separated by a Nafion® 117 cation exchange membrane (0.180 mm thick, > 0.9 meq/g exchange capacity, Alfa Aesar).

The tests are carried out with a single pass of reactants across the electrochemical reactor at current density levels of 90 and 200 mA $cm^{-2}$ for 30 min, to ensure the activity of the electrode. The concentration of formate is quantified at least by duplicate every 10 min using an ion chromatography column (Dionex ICS 1100 using $Na_2CO_3$ as eluent with a concentration of 4.5 mM and a flow rate of 1 ml $min^{-1}$). Each fabrication condition is evaluated at least twice with two different replicates to study reproducibility. Two experiments per current density are performed for every replicate, collecting three samples in each experiment. An averaged formate concentration is finally obtained for each test and used to determine the formate rate and energy consumption as defined in SI.

EIS measurements (AutoLab PGSTAT 302 N, Metrohm Hispania) are additionally carried out in the filter-press cell to electrochemically

characterize the prepared GDEs. The analyses are carried out at a constant voltage of − 0.8 V vs. Ag/AgCl and frequencies ranged between 3000 and 50 Hz to evaluate the electrochemical resistance of the surfaces.

### 2.4. Physicochemical characterization

The prepared electrodes are characterized by powder X-ray diffraction (PXRD) in a Philips X′PERT PRO automatic diffractometer operating at 40 kV and 40 mA, in theta-theta configuration, secondary monochromator with Cu-Kα radiation (λ = 1.5418 Å) and a PIXcel solid-state detector. Data are collected at RT from 5° to 70° 2θ using a step size of 0.026° and time per step of 120 s. Besides, a fixed soller of 0.5 ° and divergence slit giving a constant volume of sample illumination is used. Microstructural features of the surfaces are analysed by Scanning Electron Microscopy (SEM) using a JEOL JSM-7000 F microscope operated at 10–20 kV.

The static water contact angle for the electrode is measured by the sessile liquid drop method using a contact angle measurement system (DSA25, Krüss, Germany) to obtain information about the hydrophobicity/hydrophilicity and the wettability of the fabricated electrodes. A 2.0 μL water drop is deposited over the surface of the different layers on different sites to get an average water contact angle value, which is obtained using the software provided through image recognition.

## 3. Results and discussion

### 3.1. $CO_2$ electroreduction in a filter-press reactor

The performance of the fabricated GDEs under different manufacturing conditions is first studied for the electrocatalytic reduction of $CO_2$ to formate in the continuous filter-press reactor (see results in Table S1 and Fig. S3 as Supporting Information). Table 1 shows the electrodes and the reproducibility analyses of the manufacturing method, varying the spraying nozzle height (15 and 35 mm), step distance (1 and 3 mm), and ink flow rate (10 and 20 ml $h^{-1}$), which are evaluated at two different current density levels: 90 and 200 mA $cm^{-2}$.

The relative standard deviation (RSD) for formate rates is in general lower than 5 % for the manufactured electrodes (only higher for Electrodes 3, 5, and 12), which can be explained by the experimental error accumulated in-cell electrode testing, sample collection, and dilution, as well as ion chromatography measurements. The results clearly improve the reproducibility observed with a manual airbrushing method in previous studies, where RSD is as high as 15 % [8,11,17,23,52], thus demonstrating the benefits of the automated spray pyrolysis technique.

Subsequently, both formate rate and energy consumption for the manufactured electrodes are analysed in Figs. 1A and 1B, respectively, and compared with previous results reached under the same experimental setup and operating conditions but using a manual method for the fabrication of the electrodes [17].

First, the results at 200 mA $cm^{-2}$ show clear improvements in formate rates with respect to the manual airbrushing method [17], while no significant changes are observed when operating at 90 mA $cm^{-2}$.

According to the improved formate rates achieved at 200 mA $cm^{-2}$, the GDEs can be classified into three groups, as shown in Table 2. The first group (Group 1) significantly improves the electroreduction performance with respect to a manual fabrication method by over 15 %. Group 2 can be made up of those electrodes with an intermediate performance, exceeding the reference by around 10 %. Finally, the performance of Group 3 worsens the results obtained with the manual fabrication method.

With respect to energy consumption (Fig. 1B), GDEs in Group 1 lead to energy consumptions of around 15 % (320 kWh $kmol^{-1}$) over the reference value (277 kWh $kmol^{-1}$), showing the smallest energy consumption of all the manufactured electrodes at 200 mA $cm^{-2}$. For Group 2, energy consumption ranges from 20 % to 30 % (350–365 kWh $kmol^{-1}$) over the reference value. Finally, the worst performance group (Group 3) shows a significant increment in energy consumption of over 30 % (over 375 kWh $kmol^{-1}$). Energy consumption values have a less significant variation for 90 mA $cm^{-2}$.

Despite the complexity of linking $CO_2$ electroreduction performance with fabrication variables, some trends can be initially observed from the results displayed in Figs. 1A and 1B. The variable that shows the biggest effect on electrode performance is the spraying nozzle height, obtaining the best results for the largest nozzle height (35 mm), which can be initially attributed to a fine distribution of the catalyst particles

**Table 1**
Manufactured GDEs under different conditions.

| Electrode | Nozzle height (mm) | Step distance (mm) | Ink flowrate (ml $h^{-1}$) | Current density (mA $cm^{-2}$) | Replicate A | | Replicate B | | RSD (%) |
|---|---|---|---|---|---|---|---|---|---|
| | | | | | Formate concentration (g $L^{-1}$) | Formate rate (mmol $m^{-2}$ $s^{-1}$) | Formate concentration (g $L^{-1}$) | Formate rate (mmol $m^{-2}$ $s^{-1}$) | |
| 1 | 15 | 1 | 10 | 90 | 1.8 | 3.8 | 1.9 | 4 | 3.6 |
| | | | | 200 | 3.7 | 7.8 | 3.9 | 8.2 | 3.5 |
| 2 | 15 | 1 | 20 | 90 | 1.9 | 4 | 1.8 | 3.8 | 3.6 |
| | | | | 200 | 4.4 | 9.3 | 4.1 | 8.7 | 4.7 |
| 3 | 15 | 3 | 10 | 90 | 1.9 | 4 | 2 | 4.2 | 3.4 |
| | | | | 200 | 4.1 | 8.7 | 4.6 | 9.7 | 7.6 |
| 4 | 15 | 3 | 20 | 90 | 2 | 4.2 | 2 | 4.2 | 0 |
| | | | | 200 | 4.5 | 9.5 | 4.3 | 9.1 | 3 |
| 5 | 25 | 1 | 10 | 90 | 1.8 | 3.8 | 1.8 | 3.8 | 0 |
| | | | | 200 | 3.8 | 8 | 4.2 | 8.9 | 7.5 |
| 6 | 25 | 1 | 20 | 90 | 1.9 | 4 | 1.8 | 3.8 | 3.6 |
| | | | | 200 | 3.6 | 7.6 | 3.7 | 7.8 | 1.8 |
| 7 | 25 | 3 | 10 | 90 | 2 | 4.2 | 2 | 4.2 | 0 |
| | | | | 200 | 4.3 | 9.1 | 4.2 | 8.9 | 1.6 |
| 8 | 25 | 3 | 20 | 90 | 1.7 | 3.6 | 1.7 | 3.6 | 0 |
| | | | | 200 | 3.7 | 7.8 | 3.7 | 7.8 | 0 |
| 9 | 35 | 1 | 10 | 90 | 2 | 4.2 | 1.9 | 4 | 3.4 |
| | | | | 200 | 4.2 | 8.9 | 4.4 | 9.3 | 3.1 |
| 10 | 35 | 1 | 20 | 90 | 2 | 4.2 | 2 | 4.2 | 0 |
| | | | | 200 | 4.7 | 9.9 | 4.8 | 10.1 | 1.4 |
| 11 | 35 | 3 | 10 | 90 | 1.9 | 4 | 1.9 | 4 | 0 |
| | | | | 200 | 4.6 | 9.7 | 4.4 | 9.3 | 2.9 |
| 12 | 35 | 3 | 20 | 90 | 1.8 | 3.8 | 2 | 4.2 | 7 |
| | | | | 200 | 4.4 | 9.3 | 4.7 | 9.9 | 4.4 |

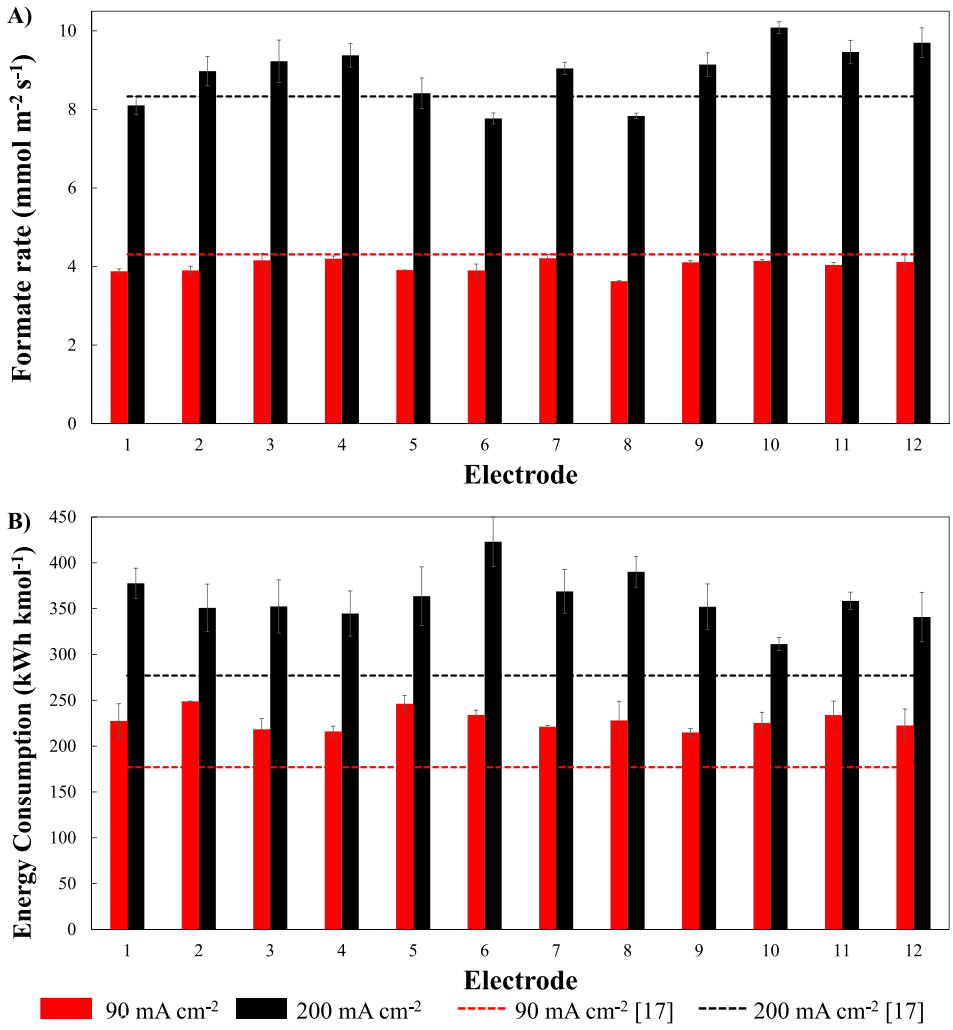


**Fig. 1.** A) Formate rates and B) Energy consumption values obtained for the herein manufactured GDEs (bar chart) compared with the mean rate values provided by the manual airbrushing (dotted lines) [17].

**Table 2**
Group of GDEs based on formate rates at 200 mA $cm^{-2}$.

| Group | Performance | Electrodes | Formate rate improvement |
|---|---|---|---|
| 1 | Best | 4, 10, 11, 12 | >15 % |
| 2 | Intermediate | 2, 3, 7, 9 | 5–10 % |
| 3 | Worst | 1, 5, 6, 8 | No improvement |

and the formation of fewer catalyst agglomerations that may reduce active area and lower charge transfer resistance [53,54]. Regarding ink flow rate, lower values show a better performance for lower nozzle heights and larger values for higher nozzle distances, which may be associated also with the fine catalyst dispersion over the electrode surface and the less formation of catalyst agglomerates under these conditions. Finally, no significant variations in formate rates can be seen with step distance.

### 3.2. Electrochemical and physicochemical characterization

To better understand the results, a representative GDE sample of each performance group is selected, Electrode 10 (Group 1), Electrode 9 (Group 2), and Electrode 8 (Group 3), for electrochemical and physicochemical characterization.

First, Fig. 2 shows the Nyquist plot obtained from impedance measurements, in comparison with a GDE fabricated with a manual airbrushing method.

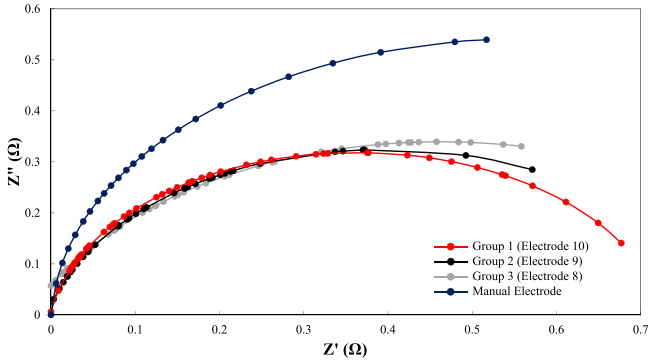


**Fig. 2.** Nyquist plots in a frequency range of 3000–50 Hz at − 0.8 V (vs. Ag/AgCl).

The impedance obtained for the automated fabrication method is reduced from that of the manual airbrushing, with an electrical resistance of 10.3 Ω $cm^2$. Comparing the selected electrodes, the lower impedance corresponds to Group 1 (Electrode 10), indicating a lower charge-transfer resistance (7.6 Ω $cm^2$) that favors formate formation rates (Fig. 1A) as a faster electrochemical reduction is expected [55]. The performance of the electrodes worsened as their electrical resistance

increased (8.1 and 9.8 Ω $cm^2$ for Groups 2 and 3, respectively) and, consequently, the energy consumption (Fig. 1B). Both electrical resistance and impedance may be related to the catalyst distribution over the GDE surface [53]. Thus, a worse catalyst dispersion over the electrode surface might cause higher electrical resistances due to the limited contact between the Bi/C nanoparticles [54], leading to a lower formate rate for Electrodes 9 and 8 (9.1 and 7.8 mmol $m^{-2}$ $s^{-1}$, respectively), together with higher energy consumption (354 and 390 kWh $kmol^{-1}$, respectively), at 200 mA $cm^{-2}$. The higher surface electrical resistivity implies a worse energy efficiency since there are losses as heat without the electrons being transferred to the reaction. Thus, this fact results in worse overall electrode performance.

According to the above inferred, SEM images (Fig. 3) reveal a fine distribution of catalytic particles in Electrode 10 (Group 1), while in Electrodes 9 and 8 the particles tend to form agglomerates that seem to lead to larger pores. This reduction in catalyst distribution may hinder the current flow, thus explaining the observed impedance increase in Fig. 2.

Furthermore, the formation of catalytic agglomerates may reduce the available surface area of the catalyst nanoparticles and the access of $CO_2$ to the catalytic active sites [54]. In this sense, a higher formate rate is obtained when a more uniform catalyst distribution over the surface is observed in Figs. 3A, 10.1 mmol $m^{-2}$ $s^{-1}$ (Fig. 1A), compared to the sample with larger surface defects (Figs. 3B and 3C), 9.2 and 7.8 mmol $m^{-2}$ $s^{-1}$ (Fig. 1A).

Moreover, electrode thickness may alter mass transfer reaction and thus play a key role in electrode behavior [56]. Fig. 4 displays the cross-sectional SEM images of the electrode samples from the three performance groups.

The images show a significant reduction in MPL thickness from the best performance electrode (Electrode 10, 75 μm) to the worst (Electrode 8, 55 μm). If we link the electrode thickness to the performance of the electrodes in the cell, it can be observed that a thicker MPL (Fig. 4A) leads to a higher formate rate of 10.1 mmol $m^{-2}$ $s^{-1}$ at 200 mA $cm^{-2}$ in comparison with the electrodes with a thinner MPL, Figs. 4B, and 4C, with rates of 9.1 and 7.8 mmol $m^{-2}$ $s^{-1}$, respectively. These results may confirm the key effect of MPL thickness on $CO_2$ electroreduction performance, which is considered a mass transfer-controlled process [57]. The better functioning of thicker MPL electrodes can be attributed to pore flooding phenomena, which takes place during electrode operation as the electrolyte clogs the electrode porous structure, affecting the hydrophobicity of the MPL due to binder degradation (usually PTFE) [58]. In this case, thicker MPLs are preferred as they avoid pore flooding, resulting in an increment of mass transfer resistance of $CO_2$ to the CL [56].

On the other hand, the MPL and CL regions can be clearly distinguished, thus demonstrating that the ink viscosity (ca 2.4 cP) prevents the presence of catalyst nanoparticles in the porous structure of the MPL [51].

Based on cross-sectional SEM images, it has been observed that the thickness of the MPL decreases from 75 to 55 μm when comparing Electrodes 10 and 8, indicating that both nozzle height and step distance have an impact on MPL thickness. Specifically, when using a lower nozzle height of 25 mm and a larger step distance of 3 mm (Electrode 8), the MPL is thinner, up to 20 μm, compared to that obtained for a nozzle height of 35 mm and a step distance of 1 mm (Electrode 10). By contrast, the ink flow rate has practically no effect on MPL thickness, as the difference between Electrodes 10 and 9 is ca 5 μm, despite varying the ink flow rate from 20 to 10 ml $h^{-1}$ under the same nozzle and step distance conditions.

### 3.3. Plasma surface post-treatment

Plasma treatment is evaluated under three different scenarios (see results in Table S2 as Supporting Information): i) treatment of the supporting Toray layer (Toray), ii) treatment of both, the supporting layer and the MPL (Toray + MPL), iii) treatment of all layers, namely the supporting layer, the MPL, and the CL (Toray + MPL + CL), as depicted in Figs. 5A and 5B.

The base electrode (Electrode 8) reaches lower formate rates compared to the electrodes where Toray + MPL and Toray + MPL + CL are treated, Fig. 5A, but no improvement is observed when only the Toray layer is treated. The most relevant enhancement (up to 12 %) is obtained when Toray + MPL are treated, obtaining a rate of 8.8 mmol $m^{-2}$ $s^{-1}$ at 200 mA $cm^{-2}$ (7.8 mmol $m^{-2}$ $s^{-1}$ for the base electrode), while the effect at 90 mA $cm^{-2}$ is less remarkable. On the other hand, no improvement can be seen when treating the CL additionally (Toray + MPL+ CL). The enhancement may be initially related to, on the one hand, the improvement of the hydrophilicity and wettability of the material [47], and, on the other hand, to the MPL thickness reduction, which may affect the $CO_2$ mass transfer resistance, facilitating the diffusion of $CO_2$ to the catalytic active sites.

Moreover, as can be seen in Fig. 5B, the energetic requirements at 200 mA $cm^{-2}$ are lowered from the base electrode (390 kWh $kmol^{-1}$) to the electrode in which Toray + MPL + CL are treated (338 kWh $kmol^{-1}$). This behavior could be associated with a drop in the charge-transfer resistance, from 9.8 Ω $cm^2$ (Base Electrode 8) to 6.7 Ω $cm^2$ for the Toray + MPL + CL treated electrode.

One of the hypotheses is that plasma treatment improves the hydrophilicity and wettability of the electrode, avoiding the clogging of the electrode pores even if they get wet, thereby promoting the three-boundary reaction in the active sites [59]. Besides, as shown in Fig. 6, plasma treatment reduces the water contact angle for every layer treated, meaning that an improvement in both surface wettability and hydrophilicity is confirmed. It is worth noting the effect of plasma in reducing the high hydrophobic character of MPL (Figs. 6B and 6E)

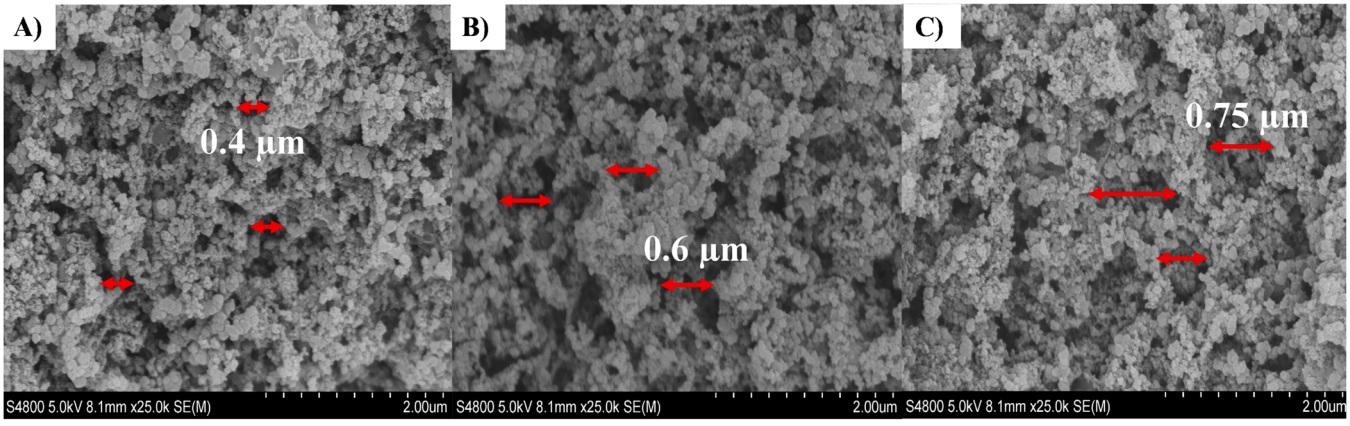


**Fig. 3.** SEM images. A) Group 1 (Electrode 10), B) Group 2 (Electrode 9), and C) Group 3 (Electrode 8).

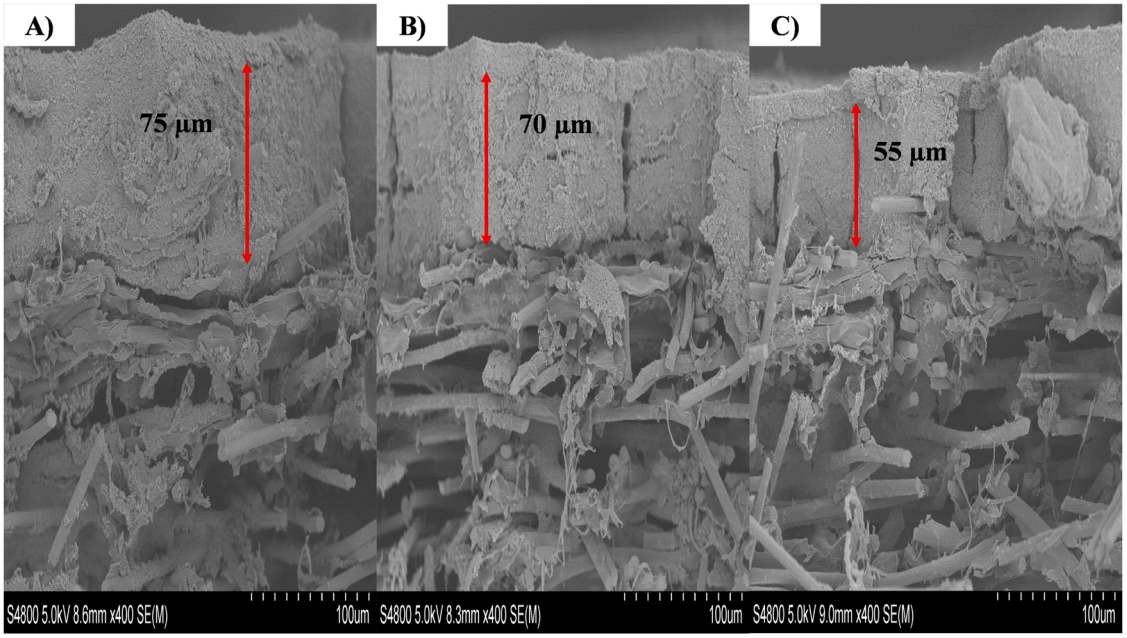


**Fig. 4.** SEM cross-section: A) Group 1 (Electrode 10), B) Group 2 (Electrode 9), and C) Group 3 (Electrode 8). Arrows depict the thickness of the MPL layer.

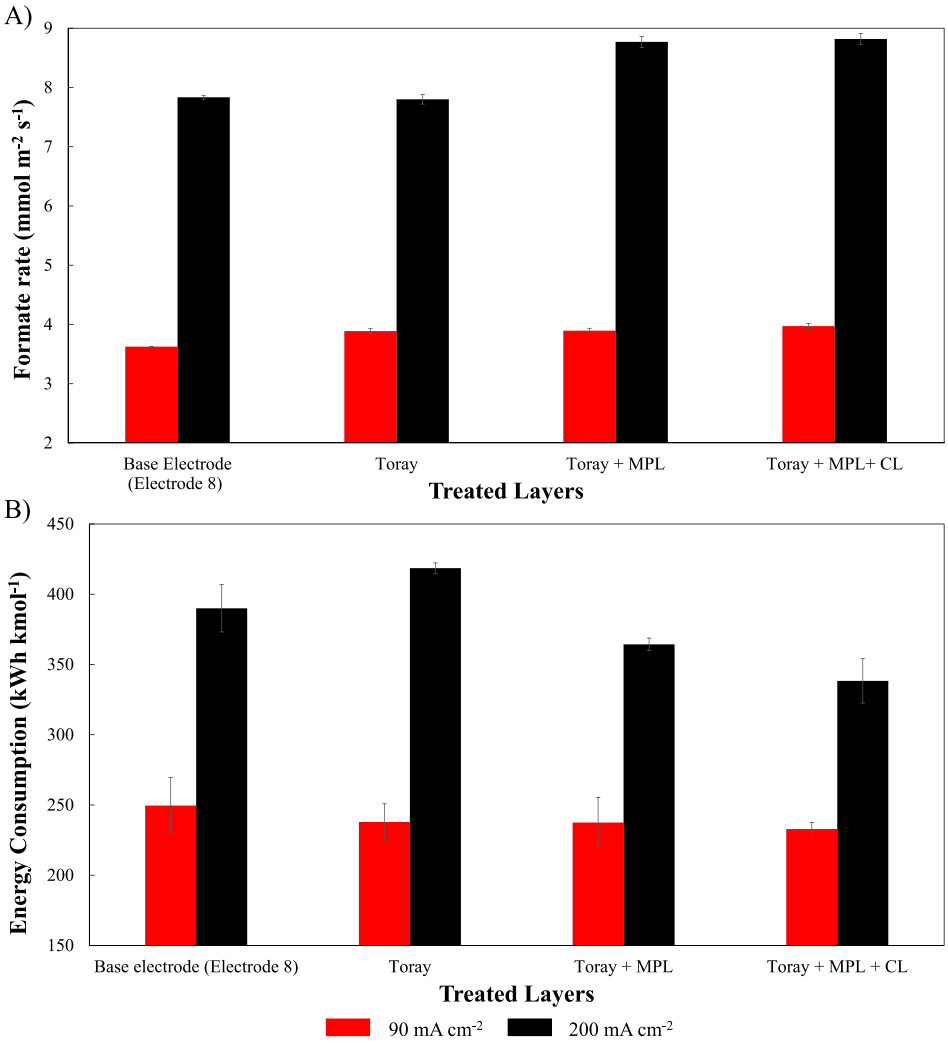


**Fig. 5.** A) Formate production rates and B) Energy consumption values for plasma-treated surfaces compared to the untreated surface (base electrode).

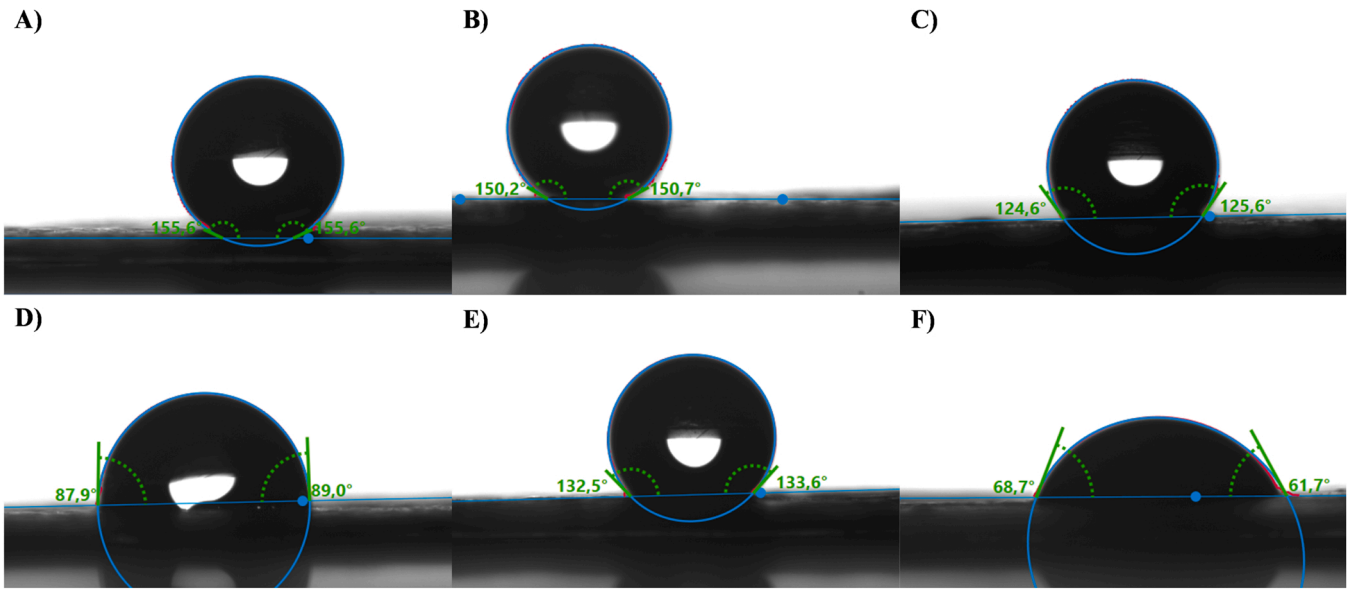


**Fig. 6.** Surface wettability assessment by the contact angle produced by a water drop over the different untreated and treated GDE layers; A) Toray layer, B) Toray + MPL layers, C) Toray + MPL + CL layers, D) Plasma treated Toray layer, E) Plasma treated Toray + MPL layers, F) Plasma treated Toray + MPL + CL layers.

caused by the presence of PTFE, from 150° to 133°. Thus, the overall reduction in the contact angle from 125° to 65° is observed when the plasma surface treatment is applied at every GDE layer (Figs. 6C and 6F).

Finally, Fig. 7 shows the plasma surface treatment effect in the internal structure of the fabricated GDEs.

The thickness of the electrode is significantly reduced (ca 20 μm) when both the MPL (Fig. 7C) and CL (Fig. 7D) layers are treated with plasma, in comparison with the untreated base electrode (Fig. 7A) and the Toray treated layer (Fig. 7B). This reduction in thickness is attributed to the bombardment of the electrode surface by active-generated compounds during the plasma treatment process [46]. Relating this to formate rate results depicted in Fig. 5A, this thickness reduction improves the electrochemical performance of the plasma-treated electrodes. As observed, the plasma-treated surfaces present higher densification that seems to be induced by a narrowing of the MPL or MPL + CL layer (Figs. 7C and 7D). This fact could improve the conductivity and avoid material losses during the reaction, consequently improving the formate rates and energy consumption, thereby confirming the trends observed in Figs. 5A and 5B. However, the contribution to mass transfer reduction due to the smaller thickness to the overall improvement may be less relevant than the improved wettability, as mass transfer resistance values are larger for the liquid phase than gas.

Besides, PXRD (Fig. S4 and Table S3, please see SI) analyses indicate that plasma treatment does not induce any changes in the reflections of crystalline phases present in the electrode, which allows for disregarding any meaningful chemical bulk changes of these materials. Hence, the improvement in electrode performance observed can still be mainly linked to the hydrophilicity of the electrode and MPL thickness.

After the analysis of the different electrodes produced by the automatic spray pyrolysis technique, Electrode 9 can be determined as the best-performance electrode in terms of formate rate (10.1 mmol $m^{-2}$ $s^{-1}$) and energy consumption (311 kWh $kmol^{-1}$), at 200 mA $cm^{-2}$, compared to the manually fabricated electrode, 8.33 mmol $m^{-2}$ $s^{-1,}$ and 277 kWh $kmol^{-1}$. The most significant variations are observed operating at 200 mA $cm^{-2}$, which is in line with Ohm's law, for high current densities, higher voltage differences occur, having a greater effect on the formate rate and energy consumption. The most favorable fabrication conditions are found for a spraying nozzle height of 35 mm, a 1 mm step

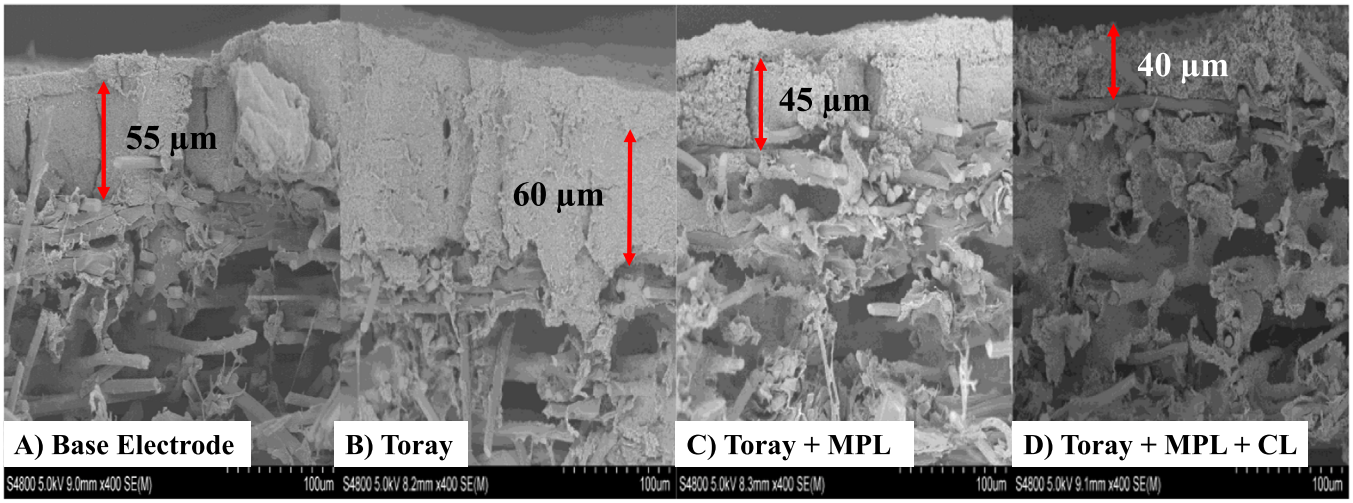


**Fig. 7.** Cross-sectional SEM images for the electrodes treated with plasma compared with the untreated Base electrode (Electrode 8). A) Base Electrode, B) Plasma treatment of the supporting Toray layer, C) Plasma treatment of the Toray and MPL, D) Plasma treatment of Toray, MPL, and CL.

distance, and a 20 ml $h^{-1}$ ink flow rate. Moreover, a plasma surface treatment can enhance formate rates and energy consumption by around 12 %, which is promoted by the improvement of the electrode wettability as demonstrated by contact angle measurements, reducing this angle by 60º, and the thickness reduction of the electrode around 10 % displayed in cross-sectional SEM images. Overall, the fabrication methodology and conditions developed in this work can be used as a standardized protocol for GDE fabrication in order to improve the reproducibility of the results in $CO_2$ electroreduction systems.

## 4. Conclusions

An electrode manufacturing process based on an automated spray pyrolysis technique coupled with a plasma surface treatment has been developed to advance toward the industrial implementation of $CO_2$ electroreduction processes. Optimal fabrication conditions of the automatic manufactured technique are found with a nozzle height of 35 mm, 1 mm of step distance, and an ink flow rate of 20 ml $h^{-1}$, obtaining the most favorable results in terms of formate rate (10.1 mmol $m^{-2}$ $s^{-1}$) and energy consumption (311 kWh $kmol^{-1}$) at 200 mA $cm^{-2}$. The electrode morphology is affected by the fabrication conditions, as both the catalyst distribution over the electrode surface and the electrode thickness are altered with different manufacturing parameters. A non-uniform catalyst distribution leads to an increment in the charge transfer resistance, over 2 Ω $cm^2$, thus affecting the reaction and lowering the formate rates achieved from 10.1 to 7.8 mmol $m^{-2}$ $s^{-1}$. On the other hand, the electrode thickness, especially the MPL thickness, plays an important role in electrode performance. A thin MPL causes pore flooding, worsening the electrode performance.

Then, a reduction in electrode thickness is observed when surfaces are treated with plasma, achieving a 10 % thinner electrode. This improvement could be mainly attributed to an enhancement in both the hydrophilicity and wettability of the electrode in which the water contact angle was reduced by 60º when plasma is applied over the Toray + MPL + CL, in comparison with the untreated electrode.

All in all, an optimized manufacturing process has been established for the fabrication of GDEs for $CO_2$ electroreduction by combining an automated spray pyrolysis technique and a plasma surface treatment. This method could be applied for manufacturing electrodes for $CO_2$ electroreduction at an industrial scale.

## CRediT authorship contribution statement

**Jose Antonio Abarca:** Conceptualization, Methodology, Validation, Investigation, Writing – original draft, Conceptualization, Data curation. **Guillermo Díaz-Sainz**: Conceptualization, Methodology, Investigation, Writing – original draft, Writing – review & editing, Supervision. **Ivan García-Merino:** Methodology, Investigation, Writing – original draft, Writing – review & editing, Supervision. **Garikoitz Beobide:** Methodology, Validation, Investigation, Writing – review & editing. **Jonathan Albo:** Conceptualization, Methodology, Writing – original draft, Writing – review & editing, Supervision, Project administration, Funding acquisition. **Angel Irabien:** Writing – review & editing, Supervision, Project administration, Funding acquisition.

## Declaration of Competing Interest

The authors declare that they have no known competing financial interests or personal relationships that could have appeared to influence the work reported in this paper.

## Data availability

No data was used for the research described in the article.

## Acknowledgements

The authors fully acknowledge the financial support received from the Spanish State Research Agency (AEI) through the projects PID2020-112845RB-I00, TED2021–129810B-C21, PID2019-104050RA-I00, and PLEC2022-009398 (MCIN/AEI/10.13039/501100011033). Jose Antonio Abarca gratefully acknowledges the predoctoral research grant (FPI) PRE2021-097200. The authors are also grateful for the nanoparticles prepared and provided by the group of Prof. V. Montiel and Dr. José Solla-Gullón from the Institute of Electrochemistry of the University of Alicante.

## Appendix A. Supporting information

Supplementary data associated with this article can be found in the online version at doi:10.1016/j.jece.2023.109724.

## References

[1] M.H. Stephenson, P. Ringrose, S. Geiger, M. Bridden, D. Schofield, Geoscience and decarbonization: current status and future directions, Pet. Geosci. 25 (2019) 501–508, https://doi.org/10.1144/petgeo2019-084.
[2] A. Mustafa, B.G. Lougou, Y. Shuai, Z. Wang, H. Tan, Current technology development for $CO_2$ utilization into solar fuels and chemicals: a review, J. Energy Chem. 49 (2020) 96–123, https://doi.org/10.1016/J.JECHEM.2020.01.023.
[3] A. Irabien, Manuel Alvarez-Guerra, J. Albo, A. Dominguez-Ramos, Electrochemical conversion of $CO_2$ to value-added products, in: C.A. Martínez-Huitle, M.A. Rodrigo, O. Scialdone (Eds.), Electrochemical Water and Wastewater Treatment, Butterworth-Heinemann, 2018, pp. 29–59.
[4] M. Ramdin, A.R.T. Morrison, M. de Groen, R. van Haperen, R. de Kler, L.J.P. van den Broeke, J.P. Martin Trusler, W. de Jong, T.J.H. Vlugt, High pressure electrochemical reduction of $CO_2$ to formic acid/formate: a comparison between bipolar membranes and cation exchange membranes, Ind. Eng. Chem. Res. 58 (2019) 1834–1847, https://doi.org/10.1021/ACS.IECR.8B04944.
[5] F. Bienen, D. Kopljar, A. Löwe, P. Aßmann, M. Stoll, P. Rößner, N. Wagner, A. Friedrich, E. Klemm, Utilizing formate as an energy carrier by coupling $CO_2$ electrolysis with fuel cell devices, Chem. Ing. Tech. 91 (2019) 872–882, https://doi.org/10.1002/CITE.201800212.
[6] S. Zhao, S. Li, T. Guo, S. Zhang, J. Wang, Y. Wu, Y. Chen, Advances in Sn-based catalysts for electrochemical $CO_2$ reduction, Nanomicro Lett. 11 (2019) 62, https://doi.org/10.1007/S40820-019-0293-X.
[7] P. Han, Z. Wang, M. Kuang, Y. Wang, J. Liu, L. Hu, L. Qian, G. Zheng, 2D assembly of confined space toward enhanced $CO_2$ electroreduction, Adv. Energy Mater. 8 (2018) 1801230, https://doi.org/10.1002/AENM.201801230.
[8] I. Merino-Garcia, L. Tinat, J. Albo, M. Alvarez-Guerra, A. Irabien, O. Durupthy, V. Vivier, C.M. Sánchez-Sánchez, Continuous electroconversion of $CO_2$ into formate using 2 nm tin oxide nanoparticles, Appl. Catal. B 297 (2021), 120447, https://doi.org/10.1016/J.APCATB.2021.120447.
[9] G. Díaz-Sainz, M. Alvarez-Guerra, A. Irabien, Continuous electroreduction of $CO_2$ towards formate in gas-phase operation at high current densities with an anion exchange membrane, J. $CO_2$ Util. 56 (2022), 101822, https://doi.org/10.1016/j.jcou.2021.101822.
[10] G. Díaz-Sainz, M. Alvarez-Guerra, J. Solla-Gullón, L. García-Cruz, V. Montiel, A. Irabien, Gas–liquid–solid reaction system for $CO_2$ electroreduction to formate without using supporting electrolyte, AIChE J. 66 (2020), e16299, https://doi.org/10.1002/AIC.16299.
[11] G. Díaz-Sainz, M. Alvarez-Guerra, B. Ávila-Bolívar, J. Solla-Gullón, V. Montiel, A. Irabien, Improving trade-offs in the figures of merit of gas-phase single-pass continuous $CO_2$ electrocatalytic reduction to formate, Chem. Eng. J. 405 (2021), 126965, https://doi.org/10.1016/j.cej.2020.126965.
[12] G. Díaz-Sainz, M. Alvarez-Guerra, J. Solla-Gullón, L. García-Cruz, V. Montiel, A. Irabien, Catalyst coated membrane electrodes for the gas phase $CO_2$ electroreduction to formate, Catal. Today 346 (2020) 58–64, https://doi.org/10.1016/J.CATTOD.2018.11.073.
[13] S. Hui, N. Shaigan, V. Neburchilov, L. Zhang, K. Malek, M. Eikerling, P. de Luna, Three-dimensional cathodes for electrochemical reduction of $CO_2$: from macro-to nano-engineering, Nanomaterials 10 (2020) 1–53, https://doi.org/10.3390/NANO10091884.
[14] N. Kumari, M.A. Haider, U. Anjum, S. Basu, Identifying operating mechanism in the electrochemical reduction of $CO_2$ on thin-film praseodymium-doped ceria electrodes, Ionics 26 (2020) 5673–5684, https://doi.org/10.1007/S11581-020-03731-1.
[15] D. Wang, S. Dong, L. Wen, W. Yu, Z. He, Q. Guo, X. Lu, L. Wang, S. Song, J. Ma, Highly selective electrocatalytic reduction of $CO_2$ to HCOOH over an in situ derived hydrocerussite thin film on a Pb substrate, Chemosphere 291 (2022), 132889, https://doi.org/10.1016/J.CHEMOSPHERE.2021.132889.
[16] I. Merino-Garcia, J. Albo, P. Krzywda, G. Mul, A. Irabien, Bimetallic Cu-based hollow fibre electrodes for $CO_2$ electroreduction, Catal. Today 346 (2020) 34–39, https://doi.org/10.1016/J.CATTOD.2019.03.025.

[17] G. Díaz-Sainz, M. Alvarez-Guerra, J. Solla-Gullón, L. García-Cruz, V. Montiel, A. Irabien, $CO_2$ electroreduction to formate: continuous single-pass operation in a filter-press reactor at high current densities using Bi gas diffusion electrodes, J. $CO_2$ Util. 34 (2019) 12–19, https://doi.org/10.1016/J.JCOU.2019.05.035.

[18] R. Kanega, N. Onishi, L. Wang, Y. Himeda, Electroreduction of carbon dioxide to formate by homogeneous ir catalysts in water, ACS Catal. 8 (2018) 11296–11301, https://doi.org/10.1021/ACSCATAL.8B02525.

[19] D. Guo, X. Wang, Z. Yang, W. Wang, H. Ning, M. Wu, Thermal driven high crystallinity of Bismuth as robust catalyst for $CO_2$ electroreduction to formate, ChemistrySelect 6 (2021) 1870–1873, https://doi.org/10.1002/SLCT.202100064.

[20] F. Cai, D. Gao, R. Si, Y. Ye, T. He, S. Miao, G. Wang, X. Bao, Effect of metal deposition sequence in carbon-supported Pd–Pt catalysts on activity towards $CO_2$ electroreduction to formate, Electrochem. Commun. 76 (2017) 1–5, https://doi.org/10.1016/J.ELECOM.2017.01.009.

[21] H. Shang, T. Wang, J. Pei, Z. Jiang, D. Zhou, Y. Wang, H. Li, J. Dong, Z. Zhuang, W. Chen, D. Wang, J. Zhang, Y. Li, Design of a single-atom indiumδ+–N4 interface for efficient electroreduction of $CO_2$ to formate, Angew. Chem. Int. Ed. 59 (2020) 22465–22469, https://doi.org/10.1002/ANIE.202010903.

[22] X. Jiang, L. Lin, Y. Rong, R. Li, Q. Jiang, Y. Yang, D. Gao, Boosting $CO_2$ electroreduction to formate via bismuth oxide clusters, Nano Res. (2022), https://doi.org/10.1007/S12274-022-5073-0.

[23] G. Díaz-Sainz, M. Alvarez-Guerra, A. Irabien, Continuous electrochemical reduction of $CO_2$ to formate: comparative study of the influence of the electrode configuration with sn and bi-based electrocatalysts, Molecules 25 (19) (2020) 4457, https://doi.org/10.3390/MOLECULES25194457.

[24] S.M. Jarvis, S. Samsatli, Technologies and infrastructures underpinning future $CO_2$ value chains: a comprehensive review and comparative analysis, Renew. Sustain. Energy Rev. 85 (2018) 46–68, https://doi.org/10.1016/J.RSER.2018.01.007.

[25] Y.Y. Birdja, E. Pérez-Gallent, M.C. Figueiredo, A.J. Göttle, F. Calle-Vallejo, M.T. M. Koper, Advances and challenges in understanding the electrocatalytic conversion of carbon dioxide to fuels, Nat. Energy 4 (2019) 732–745, https://doi.org/10.1038/S41560-019-0450-Y.

[26] M.G. Kibria, J.P. Edwards, C.M. Gabardo, C.T. Dinh, A. Seifitokaldani, D. Sinton, E. H. Sargent, Electrochemical $CO_2$ reduction into chemical feedstocks: from mechanistic electrocatalysis models to system design, Adv. Mater. 31 (2019) 1807166, https://doi.org/10.1002/ADMA.201807166.

[27] M. Rumayor, A. Dominguez-Ramos, P. Perez, A. Irabien, A techno-economic evaluation approach to the electrochemical reduction of $CO_2$ for formic acid manufacture, J. $CO_2$ Util. 34 (2019) 490–499, https://doi.org/10.1016/J.JCOU.2019.07.024.

[28] A. Gawel, T. Jaster, D. Siegmund, J. Holzmann, H. Lohmann, E. Klemm, U.P. Apfel, Electrochemical $CO_2$ reduction - the macroscopic world of electrode design, reactor concepts & economic aspects, IScience 25 (2022), 104011, https://doi.org/10.1016/J.ISCI.2022.104011.

[29] E.W. Lees, B.A.W. Mowbray, D.A. Salvatore, G.L. Simpson, D.J. Dvorak, S. Ren, J. Chau, K.L. Milton, C.P. Berlinguette, Linking gas diffusion electrode composition to $CO_2$ reduction in a flow cell, J. Mater. Chem. A. Mater. 8 (2020) 19493–19501, https://doi.org/10.1039/d0ta03570j.

[30] T. Hatsukade, K.P. Kuhl, E.R. Cave, D.N. Abram, J.T. Feaster, A.L. Jongerius, C. Hahn, T.F. Jaramillo, Carbon dioxide electroreduction using a silver–zinc alloy, Energy Tech. 5 (2017) 955–961, https://doi.org/10.1002/ENTE.201700087.

[31] F. Huq, I. Sanjuán, S. Baha, M. Braun, A. Kostka, V. Chanda, J.R.C. Junqueira, N. Sikdar, A. Ludwig, C. Andronescu, Influence of the PTFE membrane thickness on the $CO_2$ electroreduction performance of sputtered Cu-PTFE gas diffusion electrodes, ChemElectroChem 9 (2022), e202101279, https://doi.org/10.1002/CELC.202101279.

[32] E. Irtem, T. Andreu, A. Parra, M.D. Hernández-Alonso, S. García-Rodríguez, J. M. Riesco-García, G. Penelas-Pérez, J.R. Morante, Low-energy formate production from $CO_2$ electroreduction using electrodeposited tin on GDE, J. Mater. Chem. A Mater. 4 (2016) 13582–13588, https://doi.org/10.1039/C6TA04432H.

[33] Z. Miao, J. Meng, M. Liang, Z. Li, Y. Zhao, F. Wang, L. Xu, J. Mu, S. Zhuo, J. Zhou, In-situ CVD synthesis of Ni@N-CNTs/carbon paper electrode for electro-reduction of $CO_2$, Carbon 172 (2021) 324–333, https://doi.org/10.1016/J.CARBON.2020.10.044.

[34] H. Rabiee, L. Ge, X. Zhang, S. Hu, M. Li, Z. Yuan, Gas diffusion electrodes (GDEs) for electrochemical reduction of carbon dioxide, carbon monoxide, and dinitrogen to value-added products: a review, Energy Environ. Sci. 14 (2021) 1959–2008, https://doi.org/10.1039/D0EE03756G.

[35] M. Bodner, H.R. García, T. Steenberg, C. Terkelsen, S.M. Alfaro, G.S. Avcioglu, A. Vassiliev, S. Primdahl, H.A. Hjuler, Enabling industrial production of electrodes by use of slot-die coating for HT-PEM fuel cells, Int. J. Hydrog. Energy 44 (2019) 12793–12801, https://doi.org/10.1016/J.IJHYDENE.2018.11.091.

[36] T.N. Nguyen, C.-T. Dinh, Gas diffusion electrode design for electrochemical carbon dioxide reduction, Chem. Soc. Rev. 49 (2020) 7488–7504, https://doi.org/10.1039/D0CS00230E.

[37] M. Bellardita, A. di Paola, S. Yurdakal, L. Palmisano, Preparation of catalysts and photocatalysts used for similar processes, in: G. Marcì, L. Palmisano (Eds.), Heterogeneous Photocatalysis, Elsevier, 2019, pp. 25–56.

[38] S. Rahemi Ardekani, A. Sabour Rouh Aghdam, M. Nazari, A. Bayat, E. Yazdani, E. Saievar-Iranizad, A comprehensive review on ultrasonic spray pyrolysis technique: mechanism, main parameters and applications in condensed matter, J. Anal. Appl. Pyrolysis 141 (2019), 104631, https://doi.org/10.1016/j.jaap.2019.104631.

[39] B.A.W. Mowbray, D.J. Dvorak, N. Taherimakhsousi, C.P. Berlinguette, How catalyst dispersion solvents affect $CO_2$ electrolyzer gas diffusion electrodes, Energy Fuels 35 (2021) 19178–19184, https://doi.org/10.1021/ACS.ENERGYFUELS.1C01731.

[40] Q. Wang, H. Dong, H. Yu, Fabrication of a novel tin gas diffusion electrode for electrochemical reduction of carbon dioxide to formic acid, RSC Adv. 4 (2014) 59970–59976, https://doi.org/10.1039/C4RA10775F.

[41] T. Shinagawa, G.O. Larrazábal, A.J. Martín, F. Krumeich, J. Pérez-Ramírez, Sulfur-modified copper catalysts for the electrochemical reduction of carbon dioxide to formate, ACS Catal. 8 (2018) 837–844, https://doi.org/10.1021/ACSCATAL.7B03161.

[42] D. Wakerley, S. Lamaison, F. Ozanam, N. Menguy, D. Mercier, P. Marcus, M. Fontecave, V. Mougel, Bio-inspired hydrophobicity promotes $CO_2$ reduction on a Cu surface, Nat. Mater. 18 (2019) 1222–1227, https://doi.org/10.1038/s41563-019-0445-x.

[43] H. Liu, K. Xiang, Y. Liu, F. Zhu, M. Zou, X. Yan, L. Chai, Polydopamine functionalized Cu nanowires for enhanced $CO_2$ electroreduction towards methane, ChemElectroChem 5 (2018) 3991–3999, https://doi.org/10.1002/CELC.201801132.

[44] W. Ma, S. Xie, T. Liu, Q. Fan, J. Ye, F. Sun, Z. Jiang, Q. Zhang, J. Cheng, Y. Wang, Electrocatalytic reduction of $CO_2$ to ethylene and ethanol through hydrogen-assisted C–C coupling over fluorine-modified copper, Nat. Catal. 3 (2020) 478–487, https://doi.org/10.1038/s41929-020-0450-0.

[45] L. Zhang, Z. Wei, S. Thanneeru, M. Meng, M. Kruzyk, G. Ung, B. Liu, J. He, A polymer solution to prevent nanoclustering and improve the selectivity of metal nanoparticles for electrocatalytic $CO_2$ reduction, Angew. Chem. Int. Ed. 58 (2019) 15834–15840, https://doi.org/10.1002/ANIE.201909069.

[46] Y.W. Choi, F. Scholten, I. Sinev, B.R. Cuenya, Enhanced stability and CO/formate selectivity of plasma-treated $SnO_x$ /$AgO_x$ catalysts during $CO_2$ electroreduction, J. Am. Chem. Soc. 141 (2019) 5261–5266, https://doi.org/10.1021/JACS.8B12766.

[47] Y. Ma, J. Wang, J. Yu, J. Zhou, X. Zhou, H. Li, Z. He, H. Long, Y. Wang, P. Lu, J. Yin, H. Sun, Z. Zhang, Z. Fan, Surface modification of metal materials for high-performance electrocatalytic carbon dioxide reduction, Matter 4 (2021) 888–926, https://doi.org/10.1016/j.matt.2021.01.007.

[48] H. Mistry, A.S. Varela, C.S. Bonifacio, I. Zegkinoglou, I. Sinev, Y.W. Choi, K. Kisslinger, E.A. Stach, J.C. Yang, P. Strasser, B.R. Cuenya, Highly selective plasma-activated copper catalysts for carbon dioxide reduction to ethylene, Nat. Commun. 7 (2016) 12123, https://doi.org/10.1038/NCOMMS12123.

[49] D. Gao, I. Zegkinoglou, N.J. Divins, F. Scholten, I. Sinev, P. Grosse, B. Roldan Cuenya, Plasma-activated copper nanocube catalysts for efficient carbon dioxide electroreduction to hydrocarbons and alcohols, ACS Nano 11 (2017) 4825–4831, https://doi.org/10.1021/ACSNANO.7B01257.

[50] K. Jiang, Y. Huang, G. Zeng, F.M. Toma, W.A. Goddard, A.T. Bell, Effects of surface roughness on the electrochemical reduction of $CO_2$ over Cu, ACS Energy Lett. 5 (2020) 1206–1214, https://doi.org/10.1021/ACSENERGYLETT.0C00482.

[51] G. Li, T. Yan, X. Chen, H. Liu, S. Zhang, X. Ma, Electrode engineering for electrochemical $CO_2$ reduction, Energy Fuels 36 (2022) 4234–4249, https://doi.org/10.1021/ACS.ENERGYFUELS.2C00271.

[52] A. del Castillo, M. Alvarez-Guerra, A. Irabien, Continuous electroreduction of $CO_2$ to formate using Sn gas diffusion electrodes, AIChE J. 60 (2014) 3557–3564, https://doi.org/10.1002/AIC.14544.

[53] H. Rabiee, L. Ge, X. Zhang, S. Hu, M. Li, S. Smart, Z. Zhu, Z. Yuan, Shape-tuned electrodeposition of bismuth-based nanosheets on flow-through hollow fiber gas diffusion electrode for high-efficiency $CO_2$ reduction to formate, Appl. Catal. B. 286 (2021), 119945, https://doi.org/10.1016/J.APCATB.2021.119945.

[54] H.R.Q. Jhong, F.R. Brushett, P.J.A. Kenis, The effects of catalyst layer deposition methodology on electrode performance, Adv. Energy Mater. 3 (2013) 589–599, https://doi.org/10.1002/AENM.201200759.

[55] S.Y. Choi, S.K. Jeong, H.J. Kim, I.H. Baek, K.T. Park, Electrochemical reduction of carbon dioxide to formate on tin-lead alloys, ACS Sustain. Chem. Eng. 4 (2016) 1311–1318, https://doi.org/10.1021/ACSSUSCHEMENG.5B01336.

[56] Y. Wu, S. Garg, M. Li, M.N. Idros, Z. Li, R. Lin, J. Chen, G. Wang, T.E. Rufford, Effects of microporous layer on electrolyte flooding in gas diffusion electrodes and selectivity of $CO_2$ electrolysis to CO, J. Power Sources 522 (2022), 230998, https://doi.org/10.1016/J.JPOWSOUR.2022.230998.

[57] Y.C. Tan, K.B. Lee, H. Song, J. Oh, Modulating local $CO_2$ concentration as a general strategy for enhancing C−C coupling in $CO_2$ electroreduction, Joule 4 (2020) 1104–1120, https://doi.org/10.1016/J.JOULE.2020.03.013.

[58] H. Yang, Y. wen Hu, J. jie Chen, M.S.Jie T. Balogun, P. ping Fang, S. Zhang, J. Chen, Y. Tong, Intermediates adsorption engineering of $CO_2$ electroreduction reaction in highly selective heterostructure Cu-based electrocatalysts for CO production, Adv. Energy Mater. 9 (2019) 1901396, https://doi.org/10.1002/AENM.201901396.

[59] H. Rabiee, L. Ge, J. Zhao, X. Zhang, M. Li, S. Hu, S. Smart, T.E. Rufford, Z. Zhu, H. Wang, Z. Yuan, Regulating the reaction zone of electrochemical $CO_2$ reduction on gas-diffusion electrodes by distinctive hydrophilic-hydrophobic catalyst layers, Appl. Catal. B 310 (2022), 121362, https://doi.org/10.1016/J.APCATB.2022.121362.